Macromolecules
ARTICLE

Macromolecules **2009**, *42*, 7571–7578 **7571**
DOI: 10.1021/ma901157y

Tecto-Dendrimers: A Study of Covalently Bound Nanospheres

Paul M. Welch* and Cynthia F. Welch

Theoretical Division and Materials Science and Technology Division, Los Alamos National Laboratory, Los Alamos, New Mexico 87545

Received May 28, 2009; Revised Manuscript Received July 29, 2009

ABSTRACT: We present a computational and theoretical study of the size, shape, and solution properties of tecto-dendrimers. This class of polymer, composed of a central dendrimer with multiple dendrimers attached at its periphery, holds promise for multidrug delivery and environmental remediation applications. We find (i) that the maximum number of tecto-units that may be attached to the central core varies logarithmically with the ratio of the sizes of the component dendrimers, (ii) that the total density profiles display a minimum near the junction of the tecto-units with the core, (iii) that a simple expression captures the radius of gyration for a wide range of topologies, (iv) that the intrinsic viscosity displays a maximum as a function of the number of tecto-units attached, and (v) that the sphericity increases with increasing number of attached tecto-units. These results support the notion that the dendritic components can be viewed as independent building blocks for multifunctional devices.

I. Introduction

Dendrimers, with their well-defined structure and large number of potential reactive sites, hold promise as molecular building elements. Synthetic chemists have employed clever schemes for producing a number of nanostructures derived from these basic units, including dendronized polymers,[1] "dumbbell" configurations self-assembled with DNA links,[2] and tecto-dendrimers.[3−14] Tomalia and co-workers recently produced the latter by the synthetic coupling of peripheral dendrimers to a central dendritic core. The potential for multidrug delivery agents, Janus catalysts, and heavy metal remediation agents motivates efforts to produce this class of molecule. In particular, one can easily imagine combinations such as an antitumor/anticapillary cocktail delivered in a single tecto-dedrimer, as was accomplished with the polymer/lipid "nanocell" devised by Sengupta[15] and co-workers. The tecto-dendrimers, with their multiple modular components, should permit an expansion of this elegant idea.

However, several questions regarding their physics remain outstanding and potentially limit one's ability to characterize, apply, and even synthesize them. In particular, we need to understand how their detailed topological structure affects their physical properties and sets them apart from other synthetic polymers. Tecto-dendrimers may be characterized by not only their overall mass but also (like their dendrimer predecessors) the generation of growth of the dendritic units and the number of peripheral dendrimers attached to the central core. Moreover, the peripheral "tecto-units" need not be of the same generation of growth as the central dendrimer. Herein, we examine how these topological parameters dictate the number of peripheral units that can be attached, the mass distribution within the molecule, their size, their viscosity, and their sphericity.

II. Model and Algorithm

We obtained our results from a combination of analytical and computational tools. Following our previous studies,[16−19] we applied Brownian dynamics[20] to coarse-grained models of tecto-dendrimers in good solvents. The details of the simulation algorithm and model are found in ref 19; other than the topology, the model and algorithm are identical to that which we used previously in the study of dendronized polymers. We varied the generation of dendritic growth for both the central (G_C) and the tecto-units (G_T) as well as the number of attached peripheral dendrimers T and the number of beads between branch points P. Figure 1 illustrates the specific topology we studied; an example topology of $G_C = 2$, $G_T = 2$, $T = 6$, and $P = 1$ is shown alongside a snapshot from the simulations of the corresponding model. Note that one bead at each junction of tecto and central dendrimers was shared. Our study includes tecto-dendrimers composed of dendrimers whose generation of growth ranges from 2 to 6 and values of P equal to 0, 1, 3, 5, and 7. As discussed below, T was dictated by crowding and varied. The tecto-units were attached in a fashion such that they were uniformly distributed about the circumference of the two-dimensional topological map, like that shown in the left-hand side of Figure 1. Models with as many as 13 393 beads were examined. One thousand statistically independent samples were saved and analyzed from each simulation trajectory. The molecules were initially generated via a kinetic growth algorithm beginning from the central bead of the coarse-grained model. Specifically, each new bead in the molecule was placed in a random trial location one bond length away from its topological predecessor (working from the central bead of the central dendrimer outward). If the bead did not overlap any other in the molecule, the trial location was accepted. If an overlap occurred, a new position was tried. Up to 5000 new positions were tested for each bead. If an acceptable position could not be located after 5000 trials, the molecule was begun again from the first bead. Several thousand independent attempts to grow a new molecule were allowed for each. Upon the successful growth of a molecule, Brownian dynamics began. This growth algorithm is analogous to the divergent synthetic scheme, significant to the discussion below.

III. Results and Discussion

When considering these molecules, one immediately encounters a fundamental question that bears directly upon the limitations to their synthesis: what is the maximum number T_{Max} of tecto-units that can be placed around the central dendrimer?

*Corresponding author. E-mail: pwelch@lanl.gov.

Published on Web 09/04/2009

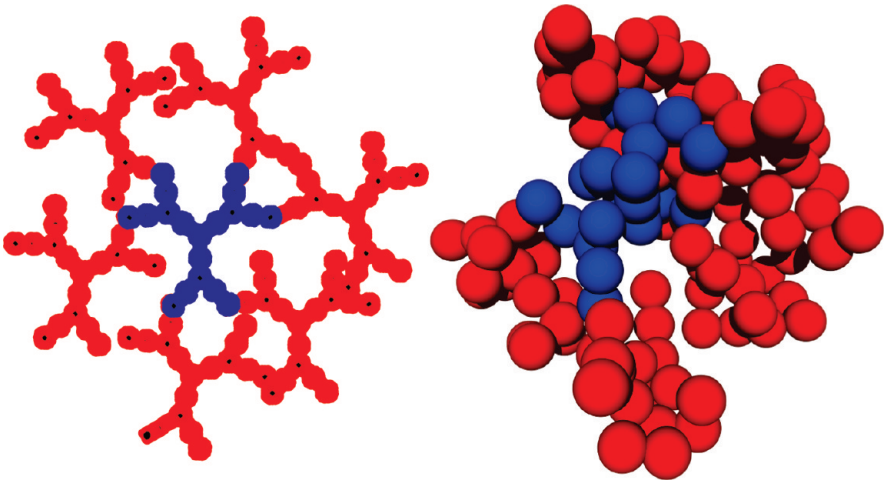

Figure 1. The image on the right illustrates a typical snapshot from the simulations. The tecto-units are shown in red while the central units are in blue. The left contains a sketch of the topology studied. Here, $G_C = 2$, $G_T = 2$, $T = 6$, and $P = 1$.

Equivalently, how many spheres of a given radius R_T can be placed around a sphere of radius R_C? This puzzle impacts not only the physics of tecto-dendrimers but also a host of other subjects, including tumor irradiation.[21] Remarkably, this seemingly straightforward question remains open. Mansfield[22] and co-workers addressed this subtle question within the context of tecto-dendrimers and found an analytical form in the limit where the central unit is much larger than the tecto-units. Specifically, they found that $T_{Max} = (2\pi/\sqrt{3})(R_C/R_T + 1)^2$, with R_C the radius of the central dendrimer and R_T the radius of an individual tecto-unit. Uppuluri[5] and co-workers found experimentally that this limit overestimates the actual number of tecto-units that can be synthetically attached via a convergent addition. Those authors discuss possible reasons for this disagreement. Here we take a more heuristic approach and arrive at an expression that covers a broader range of the size ratio than accessible to Mansfield's expression. First, we note that real synthetic dendrimers are not featureless spheres and possess a limited number T_0 of available reactive sites on which to add the tecto-units. As pointed out by Mansfield, we also know that Newton demonstrated that the maximum number of same-sized spheres that can pack around an identical sphere is 12. Thus, we direct our attention to the ratio T_{Max}/T_0 rather than simply T_{Max} and expect that, in the limit that all dendrimers are of the same size, this ratio becomes $12/T_0$. Now, we expect that in the limit that the central dendrimer is larger than the tecto-units T_{Max}/T_0 is greater than $12/T_0$ and falls off rapidly as the size ratio approaches unity. In the region where the tecto-units are larger than the central dendrimer, this ratio must be smaller than $12/T_0$ (indeed, it must ultimately reach $2/T_0$ in the utmost of this limit, but we neglect that extreme here). In agreement with these constraints, the simulations indicate that a simple logarithmic correction to Newton's result, $(T_{Max} - 12)/T_0 = \varepsilon \ln[R_C/R_T]$, captures the trend. The coefficient ε captures the rate at which the T_{Max} sites are filled and varies with the size of the central unit.

Figure 2 illustrates the validity of our estimation of T_{Max}, as determined from the exhaustive application of the kinetic growth algorithm discussed above. The graph presents all of the values of T_{Max} less than T_0. Here, we approximate R_C and R_T with the corresponding root-mean-squared radii of gyration, discussed at length below, for isolated dendrimers of the appropriate generation of growth. Tables 1−4 enumerate the values of T_{Max} found from the simulations for the various combinations of G_C, G_T, and P employed in our study. For the instances where our data set overlaps the synthetic results of Uppuluri et al., our estimates for T_{Max} greatly exceed their experimental counterparts. We posit

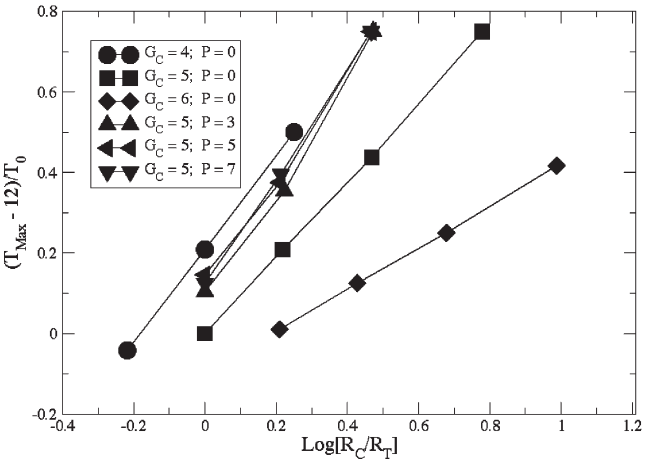

Figure 2. Simulation results for the maximum number of tecto-units attached T_{Max} plotted in accordance with our expected dependence on the ratio of the central and tecto-unit radii, R_C and R_T, respectively. Data for G_C = 4, 5, and 6 with a range of G_T values are shown. For clarity, only those points where T_{Max} began to deviate from the total possible attachment sites T_0 are included. The lines are drawn to serve as guides to the eye only.

that the primary source of this discrepancy lies in the differences in how the molecules were grown in the simulation versus the synthetic scheme. The latter relied upon a convergent growth method, attaching fully formed tecto-units to a pre-existing central dendritic core. As more tecto-units are added to the central dendrimer, this scheme undoubtedly results in slower addition kinetics as physical access to the reactive sites becomes hindered. Conversely, our simulations employed a divergent growth scheme analogous to that used in the synthesis of many dendrimers. The advantage of this approach is that at each stage of growth space must be found for only one molecular segment, not an entire dendrimer. Thus, the kinetic limitations are mitigated, and one should be able to reach the limiting values of T_{Max} in a reasonable time. We predict that this will be borne out in future synthetic studies.

We examined the mass distribution within the tecto-dendrimers to facilitate future efforts to exploit them in guest−host applications. To do this, we partitioned space around the central core of the tecto-dendrimer into a set of concentric shells. The density as a function of distance r from this central core was estimated as the average number of molecular segments found in each shell multiplied by the bead volume V_b divided by the

Table 1. Values for the Maximum Number of Attached Tecto-Units T_{max} Found in Our Simulations for $P = 0$ and 1 as a Function of the Generation of Growth for the Central (G_C) and Tecto-Units (G_T)

P	G_C	G_T	T_{Max}
0	2	2	6
		3	6
		4	6
		5	6
	3	2	12
		3	12
		4	12
		5	10
	4	2	24
		3	24
		4	17
		5	11
	5	2	48
		3	33
		4	22
		5	12
	6	2	52
		3	36
		4	24
		5	13
1	5	5	15

Table 2. Values for the Maximum Number of Attached Tecto-Units T_{max} Found in Our Simulations for $P = 3$ as a Function of the Generation of Growth for the Central (G_C) and Tecto-Units (G_T)

P	G_C	G_T	T_{Max}
3	2	2	6
		3	6
		4	6
		5	6
	3	2	12
		3	12
		4	12
		5	12
	4	2	24
		3	24
		4	24
		5	17
	5	2	48
		3	48
		4	29
		5	17

volume of each shell. Figure 3 contains the density profile for the central dendrimer segments, $\rho_C(r)$, with $G_C = 6$, $P = 0$, and various numbers of attached tecto-units with $G_T = 5$. As found in nearly every computational study of dendritic molecules to date, a radially decaying profile describes ρ_C.[23] We also note that, independent of the number or generation of growth of the tecto-units added, the central dendrimer's density profile remains unaltered, and the tecto-units do not appear to significantly penetrate the central dendrimer. While we find this impenetrability in the range of P and G values studied here, the more open structures that should arise with much larger values of P (or lower values of G combined with intermediate values of P) likely do interpenetrate. That the different dendrimers remain segregated in our present study can be clearly seen from the simulation snapshots. Figure 4 contains an example from simulations of a $G_C = 5$, $G_T = 5$, $P = 7$, $T = 12$ molecule (all units are the same but are colored differently to illuminate this effect). Indeed, examining the density profile of the entire molecule, $\rho(r)$, reveals a slight minimum in the total density profile at the junction of the central and tecto-units. This is illustrated in Figure 5 for a set of molecules with $P = 0$, $G_C = 6$, and varying number of $G_T = 5$ tecto-units. Note that the minimum becomes more pronounced as the number of tecto-units T increases. The effect on $\rho(r)$ of increasing P to larger values is discussed in detail below.

Table 3. Values for the Maximum Number of Attached Tecto-Units T_{max} Found in Our Simulations for $P = 5$ as a Function of the Generation of Growth for the Central (G_C) and Tecto-Units (G_T)

P	G_C	G_T	T_{Max}
5	2	2	6
		3	6
		4	6
		5	6
	3	2	12
		3	12
		4	12
		5	12
	4	2	24
		3	24
		4	24
		5	16
	5	2	48
		3	48
		4	30
		5	19

Table 4. Values for the Maximum Number of Attached Tecto-Units T_{max} Found in Our Simulations for $P = 6$ as a Function of the Generation of Growth for the Central (G_C) and Tecto-Units (G_T)

P	G_C	G_T	T_{Max}
7	2	2	6
		3	6
		4	6
		5	6
	3	2	12
		3	12
		4	12
		5	12
	4	2	24
		3	24
		4	24
		5	17
	5	3	48
		4	48
		5	31
		5	18

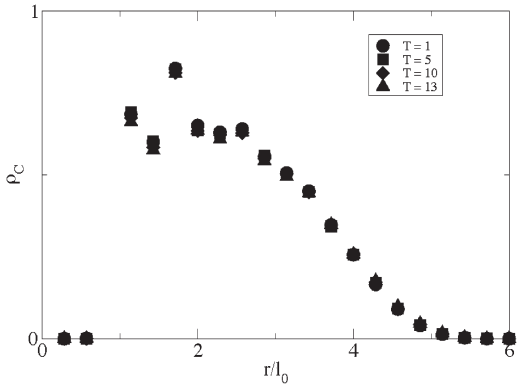

Figure 3. Radial density profile of the central dendrimer unit, ρ_C, as a function of the distance from the topological center of the molecule, r. Data for $G_C = 6$, $G_T = 5$, and $P = 0$ are shown.

Figure 6 contains a plot of the total contribution ρ_T to $\rho(r)$ due to the tecto-units for a series of $G_C = 6$, $G_T = 5$, and $P = 0$ molecules with varying values of T. Two traits stand out from the plot. First, the range of distances from the center of the tecto-dendrimer where there is appreciable density due to the tecto-units is independent of T. Second, increasing T produces a corresponding increase in the peak magnitude of ρ_T. These facts and the observed segregation thus imply that ρ_T is approximately T times the density profile of any single tecto-unit in the molecule ${}^0\rho_T$.

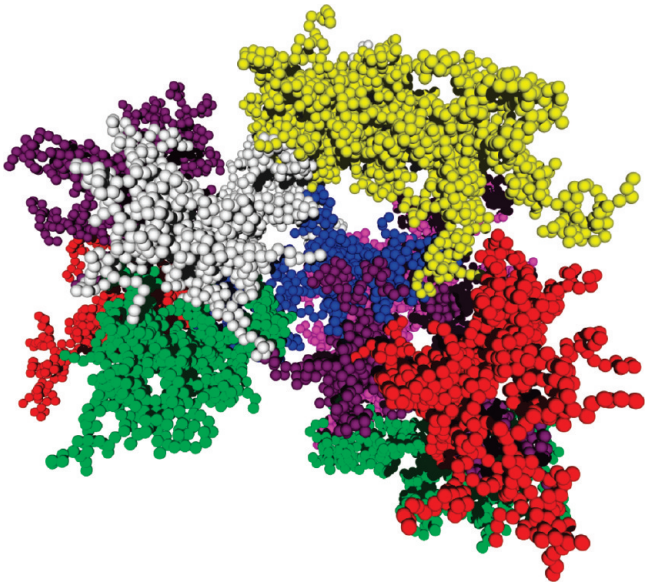

Figure 4. Snapshot from the simulation of a $G_C = 5$, $G_T = 5$, $P = 7$, and $T = 12$ tecto-dendrimer. All of the units are the same but are colored differently for contrast.

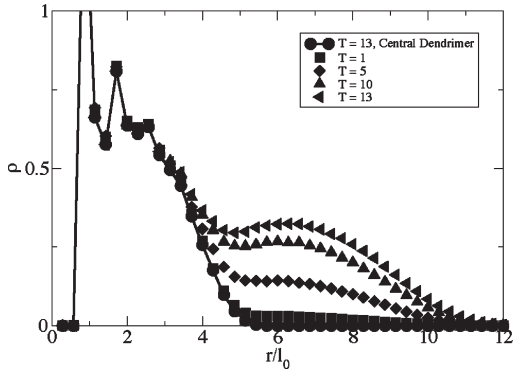

Figure 5. Radial density profile of the entire tecto-dendrimer, ρ, for $G_C = 6$, $G_T = 5$, $P = 0$, and a range of T values, superimposed upon the density profile of the central dendrimer ρ_C for $G_C = 6$, $G_T = 5$, $P = 0$, and $T = 13$.

Indeed, normalizing ρ_T by T very nearly collapses the data onto a single curve, as shown in Figure 7.

Figure 8 presents ρ as a function of the radial distance from the center for $G_C = 5$, $G_T = 5$, and $T = 12$. From these plots, one can clearly see that the local minimum in ρ is most pronounced at lower values of P. This does not, however, imply that there is substantial overlap of the tecto-units with the central unit at the higher values of P studied here. That there is segregation between the dendritic units can be directly observed from examination of the snapshots, as seen in Figure 4. This trend does, however, imply a more open and diffuse structure for larger values of P.

Thus informed about the mass distribution, we relate the squared radius of gyration $\langle R_g^2 \rangle$ of a tecto-dendrimer to the number of tecto-units T, the mass of the central unit N_C, and the mass of a single tecto-unit N_T by a simple argument. Figure 9 contains a plot of $\langle R_g^2 \rangle^{1/2}$ normalized by the bond length l_0 versus the total mass of the molecule $M = N_C + TN_T$ for 30 different combinations of P, G_C, and G_T. Statistics on $\langle R_g^2 \rangle^{1/2}$ were collected on all combinations of G_C and G_T listed in Tables 1−4 for $P = 0$, while only molecules with $G_C = 5$ were examined for topologies with $P > 0$. The different symbols represent the different combinations of G_C and P. Different

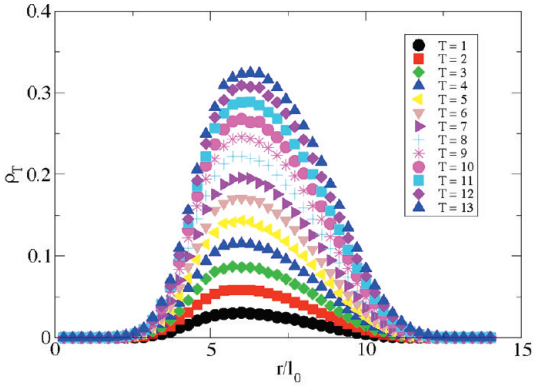

Figure 6. Radial density profile of the tecto-units only, ρ_T. Data for $G_C = 6$, $G_T = 5$, and $P = 0$ are shown.

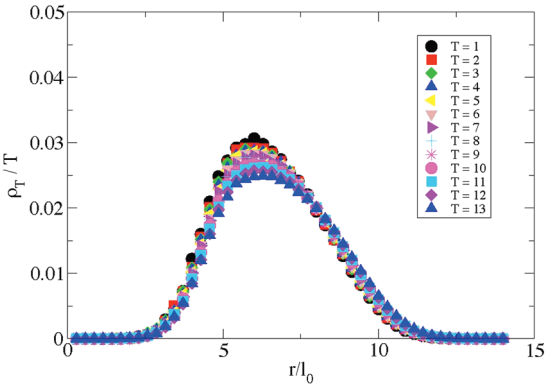

Figure 7. Radial density profile of the tecto-units ρ_T normalized by T. Data for $G_C = 6$, $G_T = 5$, and $P = 0$ are shown.

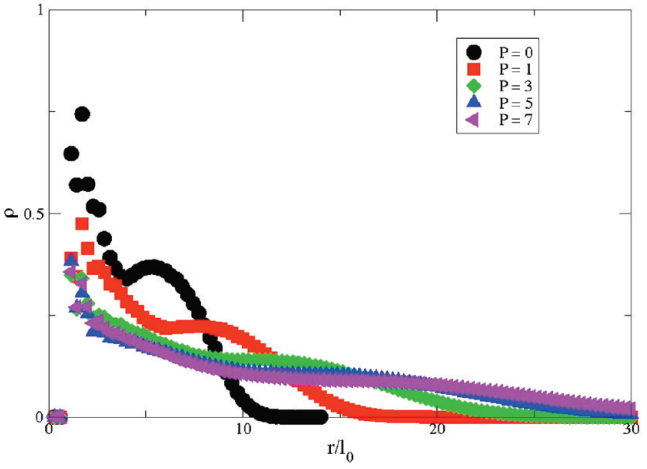

Figure 8. Radial density profile of the entire tecto-dendrimer ρ as a function of five different values of P. Data for $G_C = 5$, $G_T = 5$, and $T = 12$ are shown.

colors are used for each value of G_T. Clearly, despite some qualitative features common among the curves, each parameter combination results in an independent trend. However, a straightforward analysis reveals the underlying relationships.

One may calculate $\langle R_g^2 \rangle$ by using the mass distribution ρ as

$$\langle R_g^2 \rangle = \frac{\int d\vec{R}\, (\vec{R} - \vec{R}_{com})^2 \rho(\vec{R})}{\int d\vec{R}\, \rho(\vec{R})}$$

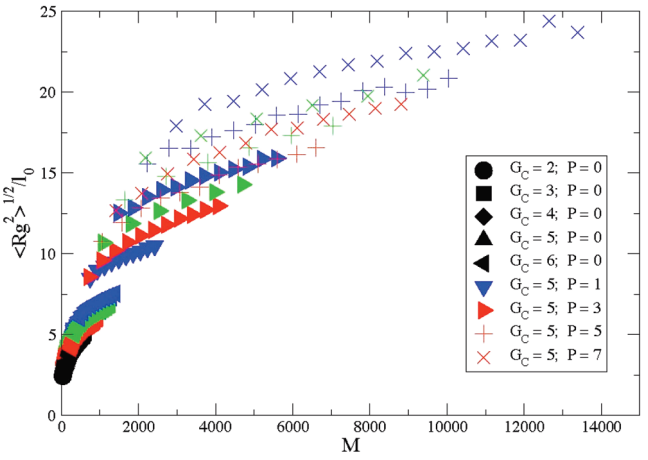

Figure 9. Simulation results for the root-mean-squared radius of gyration $\langle R_g^2\rangle^{1/2}$ plotted as a function of the total mass of the tecto-dendrimer, $M = N_C + TN_T$. Data for a range of G_C, G_T, P, and T are shown. The shape of the symbol represents the combination of G_C and P (as indicated in the legend), while the color represents the value of G_T (black for $G_T = 2$, red for $G_T = 3$, green for $G_T = 4$, and blue for $G_T = 5$).

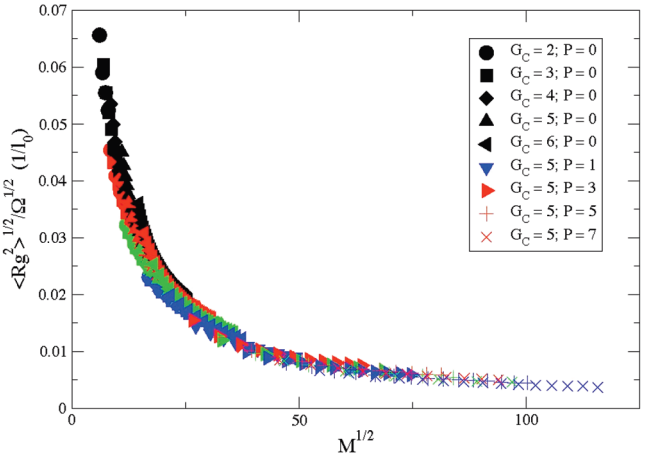

Figure 10. Simulation results for the root-mean-squared radius of gyration $\langle R_g^2\rangle^{1/2}$ divided by $\Omega^{1/2}$ (as defined in the text) plotted in accordance with our predicted dependence on the square root of the molecular mass $(N_C + TN_T)^{1/2}$. As in Figure 9, data for a range of G_C, G_T, P, and T are shown. The shape of the symbol represents the combination of G_C and P (as indicated in the legend), while the color represents the value of G_T (black for $G_T = 2$, red for $G_T = 3$, green for $G_T = 4$, and blue for $G_T = 5$).

Here, $\vec{R}_{com}$ is the center of mass of the molecule, which we assume is always located at the center of the central unit. Further assuming spherical symmetry reduces the 3-D integral to

$$\langle R_g^2\rangle = \frac{\int_0^\infty dr\, r^4\rho(r)}{\int_0^\infty dr\, r^2\rho(r)}$$

Now, as discussed above, the tecto-units do not appreciably penetrate the central unit. This allows us to further decompose the integrals into two regions by noting that $\rho(r) = \rho_C(r)$ for r less than the maximum extent of the central dendrimer, R_C. Similarly, we approximate $\rho(r) = T\,{}^0\rho_T(r)$ for r greater than R_C but less than the maximum extent of the entire molecule R_M. Thus, we find that we must evaluate four integrals:

$$\langle R_g^2\rangle = \frac{\int_0^{R_C} dr\, r^4\rho_C(r) + \int_{R_C}^{R_M} dr\, r^4 T\,{}^0\rho_T(r)}{\int_0^{R_C} dr\, r^2\rho_C(r) + \int_{R_C}^{R_M} dr\, r^2 T\rho_T(r)}$$
$$= \frac{V_b\langle R_g^2\rangle_C N_C + 4\pi\int_{R_C}^{R_M} dr\, r^4 T\,{}^0\rho_T(r)}{V_b N_C + V_b T N_T}$$

The first integral in the numerator is the un-normalized squared radius of gyration of the central dendrimer, $\langle R_g^2\rangle_C$. The sum of the two integrals in the denominator is proportional to the total mass of the molecule. The bead volume V_b terms are needed to maintain consistency with our definition of ρ above.

The remaining integral is nontrivial to evaluate. However, we make progress by applying the "Flory" argument due to Sheng and co-workers for dendrimers.[24] Those authors found that dendrimers obey a simple relationship between their mass N, generation of growth G, spacer P, and their size, $\langle R_g^2\rangle = \alpha N^{2/5} G^{4/5} (P+1)^{4/5}$. The proportionality constant α carries units of length squared. Thus, $R_M = \alpha^{1/2}(P+1)^{2/5}[2N_T{}^{1/5}G_T{}^{2/5} + N_C{}^{1/5}G_C{}^{2/5}]/\gamma$, the sum of the absolute radius of the central unit and the diameter of a tecto-unit. The ratio γ of the radius of gyration to the absolute radius depends upon the mass distribution within a molecule. Next, we approximate $T\,{}^0\rho_T(r) \approx TN_T V_b/[{}^4/_3\pi(R_M{}^3 - R_C{}^3)]$; note that for our dendrimer models $\gamma \approx 0.69$, and the integral becomes trivial to evaluate. The specific value of γ for our model was found by comparing the maximum extent of the density profile to $\langle R_g^2\rangle^{1/2}$ for the corresponding dendrimer. It is intermediate between that expected for a simple solid sphere (flat density profile) and that for a sphere with a purely decaying density profile.[25] We arrive at $\langle R_g^2\rangle = \alpha\Omega/M$. The coefficient Ω is given by $\Omega = [N_C{}^{7/5}G_C{}^{4/5}(P+1)^{4/5} + KT\beta]$. Note that Ω contains all of the topological information about the tecto-dendrimers. The constant

$$K = \frac{3}{5\gamma^2} \approx 1.26$$

and

$$\beta = N_T(P+1)^{4/5}\frac{[2N_T{}^{1/5}G_T{}^{2/5} + N_C{}^{1/5}G_C{}^{2/5}]^5 - N_C G_C{}^2}{[2N_T{}^{1/5}G_T{}^{2/5} + N_C{}^{1/5}G_C{}^{2/5}]^3 - N_C{}^{3/5}G_C{}^{6/5}}$$

again taking advantage of the scaling results of Sheng.

Figure 10 presents a plot of the simulation results for all 30 data sets contained in Figure 9, which includes all simulation results for $T > 2$. The results are presented with the root-mean-square radius of gyration normalized by Ω, capturing the connectivity, varying as a function of the square root of the total mass. By dividing by Ω, we remove the differences in the radius of gyration due to the different topologies. As expected, all of the data fall on essentially a single curve except for those points representing low values of T. This systematic deviation at low T values derives from the breakdown of the assumption that the center of the central dendrimer lies coincident with the center of mass. Conversely, the success of this simple approach proves the veracity of the central assumption employed: the different dendritic units do not interpenetrate and may be treated as independent building blocks.

Note that our prediction for $\langle R_g^2\rangle^{1/2}$ indicates that the size of the molecule initially rises rapidly with increasing number of tecto-units T but then reaches an asymptotic limit. This is also reflected in Figure 9, as the curve rolls over and begins to flatten at higher values of T. Conversely, the total mass of the molecule continues to rise linearly with increasing T. This suggests that a curious trend should be observed when the intrinsic viscosity $[\eta]$ is plotted as a function of T. Typical linear polymers display a power-law increase in $[\eta]$ with increasing molecular weight. However, dendrimers (as opposed to tecto-dendrimers) exhibit

a peak in $[\eta]$ as a function of their generation of growth G.[26,27] This can be understood by appealing to the well-known relation between the intrinsic viscosity and the ratio of the hydrodynamic volume $^4/_3\pi R_H^3$ to molecular mass M, $[\eta] \propto R_H^3/M$. This scaling law is easily obtained from the Einstein relation between viscosity and volume fraction and underlies the familiar Mark−Houwink expression relating intrinsic viscosity to molecular weight.[28] While the mass grows exponentially with G, the radius grows more slowly in dendrimers. Giupponi and Buzza[29] demonstrated that the scaling law due to Sheng and co-workers best captures this behavior. Similarly, we predict that $[\eta]$ for the tecto-dendrimers will also exhibit a maximum when plotted as a function of T. Again, $[\eta]$ will vary directly with the cubed radius of the molecule and inversely with the mass. The radius will reach an asymptotic value as T is increased, but the mass will continue to grow (albeit linearly) with T. To test this, we employed the estimate $[\eta] \propto R_H^3/M$, where R_H is the hydrodynamic radius obtained by applying the numerical path integration technique due to Mansfield, Douglas, and Garboczi.[30] Within this method, one appeals to the mathematical similarities between hydrodynamics and electrical polarizability. For this study, we employed the program Zeno[31] to calculate R_H, as averaged over all of our snapshots. Other dynamical methods such as that applied by Bosko and Prakash[32] could be employed, but this more economical method has also proven successful for dendritic[30] molecules. Figure 11 contains the simulation predictions for R_H^3/M as a function of T for $G_C = 6$, $P = 0$, and various values of G_T. Similar results were found for higher values of P, with R_H^3/M shifting to correspondingly higher values. The predicted peak occurs and becomes more pronounced with increasing values of G_T. To our knowledge, this prediction has not yet been observed or tested experimentally.

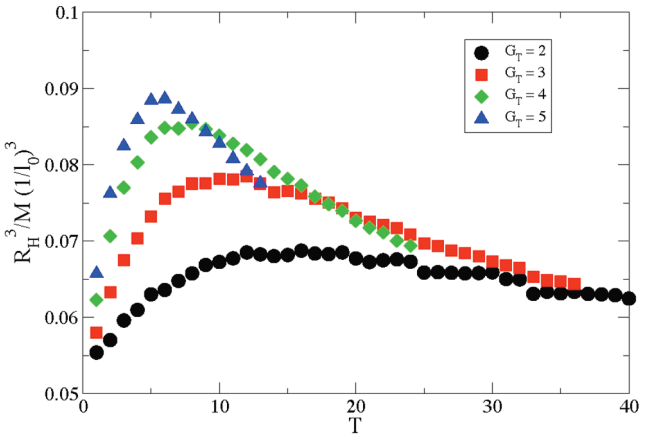

Figure 11. Estimated trends for the intrinsic viscosity as approximated from the ratio of the hydrodynamic radius cubed R_H^3 to the total molecular mass $(N_C + TN_T)$. Data from $G_C = 6$ and $P = 0$ are shown.

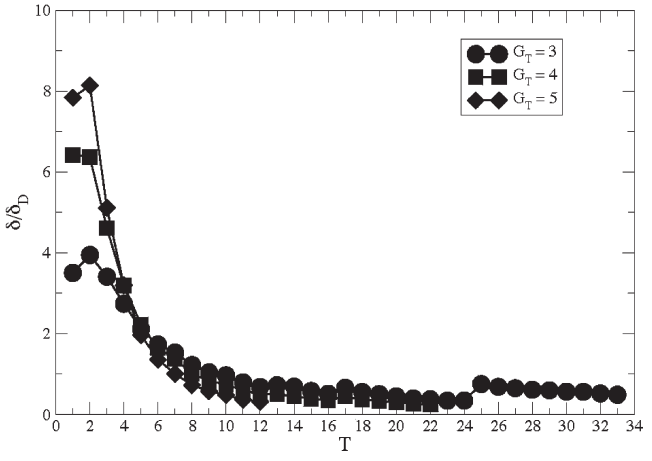

Figure 12. Normalized sphericity δ/δ_D as a function of T for $G_C = 5$ and $P = 0$ topologies.

Many of the proposed applications of tecto-dendrimers require that they interact with biological membranes. Experimental studies by Mecke[33] and co-workers demonstrate that dendrimers create holes in lipid bilayers while tecto-dendrimers do not. Specifically, they considered PAMAM and a $G_C = 7$, $G_T = 5$, $T = 10-12$ PAMAM-based tecto-dendrimer. They postulate that the lipids form a stable bilayer vesicle around the approximately spherical dendrimers but cannot do so to surround the less spherical tecto-dendrimers. This leads to poor association between the tecto-dendrimers and the lipids. If this postulate is correct, sphericity may play a major role in determining the bioavailability of tecto-dendrimers.

In order to quantify sphericity as a function of the various topological parameters, we follow the work of Rudnick and Gaspari.[34] The shape tensor $S_{\alpha\beta}$ for an arbitrary molecule is given by

$$S_{\alpha\beta} = \frac{1}{M}\left[\sum_{i=1}^{M}(r_{\alpha,i} - r_{\mathrm{com},\alpha})(r_{\beta,i} - r_{\mathrm{com},\beta})\right]$$

where α and β represent the x, y, or z components of the bead position $\mathbf{r}$ and center of mass $\mathbf{r}_{com}$. The three eigenvalues of this tensor s_1, s_2, and s_3 yield a quantitative measure of sphericity $\delta = 1 - 3\langle I_2\rangle/\langle I_1^2\rangle$ with $I_1 = s_1 + s_2 + s_3$ and $I_2 = s_1s_2 + s_2s_3 + s_3s_1$. This function approaches 0 for a sphere and 1 for a cigar-shaped

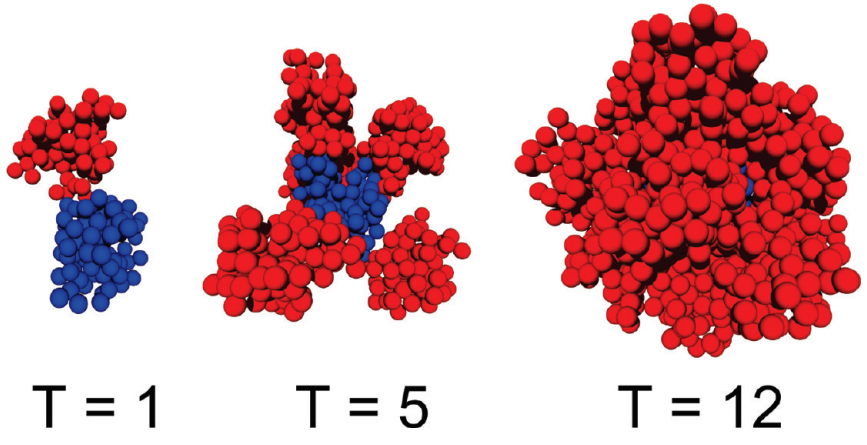

Figure 13. Typical snapshots from simulations of $G_C = 5$, $G_T = 5$, $P = 0$ tecto-dendrimers with three different values of T.

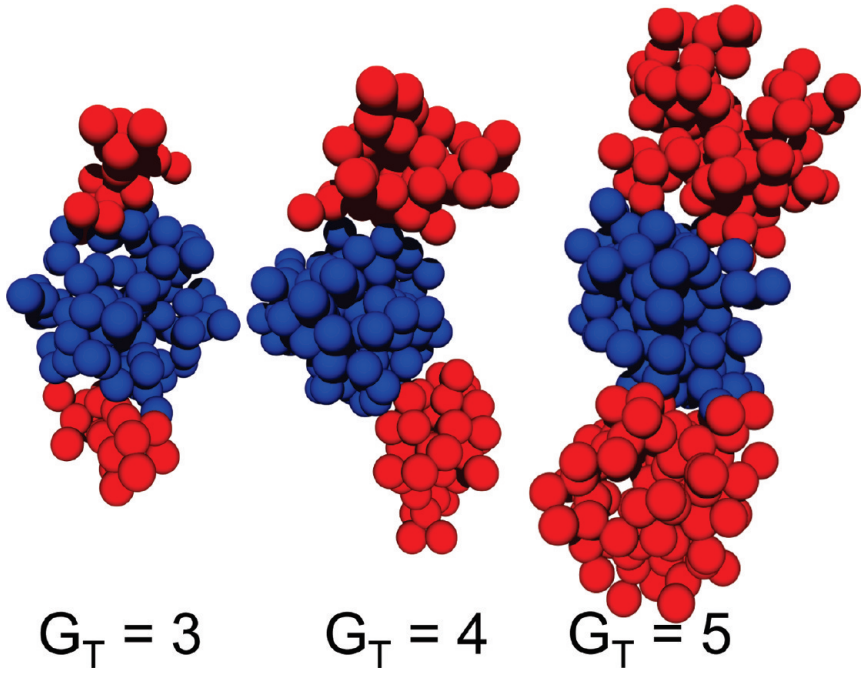

Figure 14. Typical snapshots from simulations of $G_C = 5$, $T = 2$, $P = 0$ tecto-dendrimers with three different values of G_T shown.

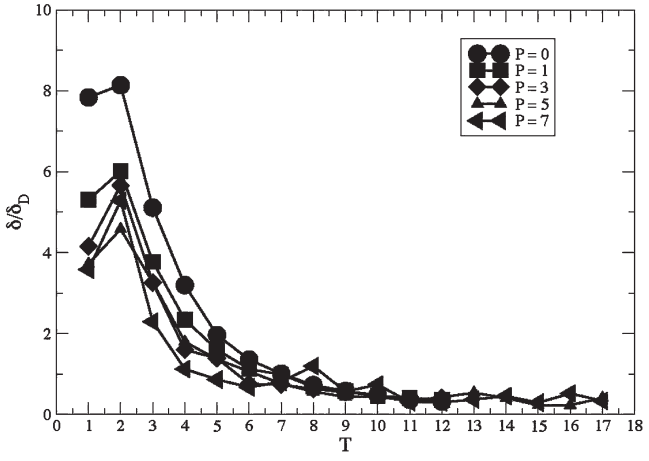

Figure 15. Normalized sphericity δ/δ_D as a function of T for $G_C = 5$ and $G_T = 5$ topologies with varying P values.

object. We find that the apparent sphericity of our model tecto-dendrimers depends upon the relative sizes of the central dendrimer and the tecto-units, but more strongly upon the number of tecto-units attached. Figure 12 contains a plot of normalized δ values as a function of T for $G_C = 5$ and $P = 0$ for three different values of G_T. The normalization δ_D is the sphericity of a generation 5, $P = 0$ dendrimer. Several traits are evident from the curve. Clearly, increasing T increases the sphericity, as one would expect. One can easily see this upon examining the snapshots from the simulations, as pictured in Figure 13 for a series of $G_C = 5, G_T = 5$, and $P = 0$ tecto-dendrimers. For all three of the G_T values presented Figure 12, the ratio δ/δ_D falls below 1 around $T = 7-10$, indicating that the tecto-dendrimers may actually exceed the sphericity of a corresponding dendrimer. However at the lower values of T, there is a dramatic increase in the ratio, including a maximum at $T = 2$, the most oblong topology. We also note that increasing the value of G_T produces a corresponding increase in δ/δ_D in this region; again, snapshots from the simulations of $G_C = 5$, $P = 0$ tecto-dendrimers with $G_T = 3, 4$, and 5 illustrate this qualitatively, as pictured in Figure 14. Similar

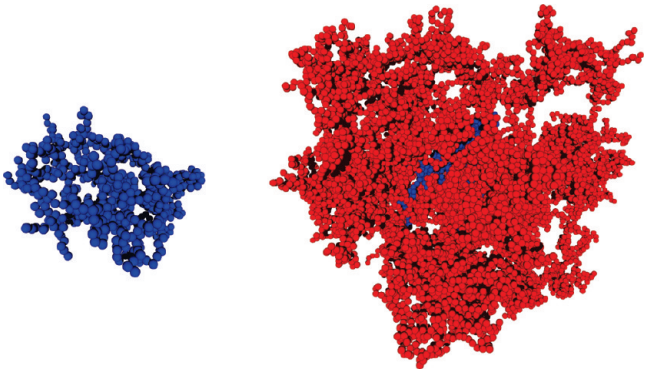

Figure 16. Typical snapshots from simulations of a generation 5 dendrimer with $P = 7$ (left) and a $G_C = 5$, $G_T = 5$, $T = 17$, and $P = 7$ tecto-dendrimer (right).

trends for the dependence upon T manifest at higher values of P, as shown in Figure 15 for $G_C = 5$ and $G_T = 5$ tecto-dendrimers with a range of P values. There, the data are normalized by δ_D for a generation 5 dendrimer with the corresponding P values. As for the $P = 0$ data, all of the tecto-dendrimers become at least as spherical as their respective dendrimers for values of T in excess of 7. This can be clearly seen in Figure 16, which contains snapshots for a generation 5 dendrimer and a $G_C = 5, G_T = 5, T = 17$ tecto-dendrimer, both with $P = 7$.

IV. Conclusions

In summary, our analytical and computational studies of tecto-dendrimers yield several predictions that should impact both their synthesis and application. Though variegated, we find that their dimensions and the limits to their synthesis succumb to relatively simple theoretical predictions embodied in the equations above. Our computational estimates for the maximum number of tecto-units that can be attached exceed that realized in convergent synthetic schemes, suggesting that a divergent scheme (doubtlessly more difficult to devise) may result in a greater number of linked tecto-units. They present a minimum in their density profile near the junction of the central- and

tecto-units, a property that may play a role in future guest−host applications. Relying upon the Flory argument of Sheng and the assumption that the dendritic subunits do not interpenetrate, we arrive at an expression for predicting the dependence of the size of the molecule upon its various topological parameters. The success of that equation further supports the notion that the individual dendritic components may be viewed as independent building blocks with which to construct multifunctional molecular species. The expression also predicts that the size of the molecule grows asymptotically with the number of attached tecto-units. This suggests that the intrinsic viscosities of the materials will display an unusual peak with increasing number of tecto-units attached, a trait analogous to that observed in dendrimers. This is supported by the estimation of the trend in the intrinsic viscosities from the simulations and should be easily tested by experimental measurements. Finally, we note that the sphericity of the tecto-dendrimers depends upon the number of tecto-units attached in a nonmonotonic fashion, reaching a low when only two tecto-units are present. However, we also find that the sphericity quickly matches that of dendrimers after the addition of around 7−10 tecto-units. In light of the experimental work by Mecke and company, this suggests that their bioavailability may be tuned by varying the number of tecto-units present.

Acknowledgment. This work was carried out under the auspices of the National Nuclear Security Administration of the U.S. Department of Energy at Los Alamos National Laboratory under Contract DE-AC52-06NA25396. Financial support provided by the U.S. Department of Energy Office of Biological and Environmental Research under Proposal SCFY081004.

References and Notes

(1) For example, see: Percec, V.; Ahn, C.-H.; Ungar, G.; Yeardly, D. J. P.; Möller, M.; Sheiko, S. S. *Nature* **1998**, *391*, 161. Fréchet, J. M. J. *Macromolecules* **2006**, *39*, 476.
(2) Choi, Y.; Mecke, A.; Orr, B. G.; Holl, M. M. B.; Baker, J. R. *Nano Lett*. **2004**, *4*, 391. De Mattei, C. R.; Huang, B.; Tomalia, D. A. *Nano Lett*. **2004**, *4*, 771l.
(3) Li, J.; Swanson, D. R.; Qin, D.; Brothers, H. M.; Piehler, L. T.; Tomalia, D.; Meier, D. J. *Langmuir* **1999**, *15*, 7347.
(4) Tomalia, D. A.; Uppuluri, S.; Swanson, D. R.; Li, J. *Pure Appl. Chem*. **2000**, *72*, 2343.
(5) Uppuluri, S.; Swanson, D. R.; Piehler, L. T.; Li, J.; Hagnauer, G. L.; Tomalia, D. A. *Adv. Mater*. **2000**, *12*, 796.
(6) Baker, J. R.; Quintana, A.; Piehler, L.; Banazak-Holl, M.; Tomalia, D.; Raczka, E. *Biomed. Microdevices* **2001**, *3*, 61.
(7) Tomalia, D. A. *High Perform. Polym*. **2001**, *13*, S1.
(8) Tomalia, D. A.; Brothers II, H. M.; Piehler, L. T.; Durst, H. D.; Swanson, D. R. *Proc. Natl. Acad. Sci. U.S.A*. **2002**, *99*, 5081.
(9) Betley, T. A.; Hessler, J. A.; Mecke, A.; Holl, M. M. B.; Orr, B. G.; Uppuluri, S.; Tomalia, D. A.; Baker, J. R. *Langmuir* **2002**, *18*, 3127.
(10) Patri, A. K.; Majoros, I. J.; Baker, J. R. *Curr. Opin. Chem. Biol*. **2002**, *6*, 466.
(11) Khopade, A. J.; Möhwald, H. *Macromol. Rapid Commun*. **2005**, *26*, 445.
(12) Shi, X.; Patri, A. K.; Lesniak, W.; Islam, M. T.; Zhang, C.; Baker, J. R.; Balogh, L. P. *Electrophoresis* **2005**, *26*, 2960.
(13) Tomalia, D. A. *Prog. Polym. Sci*. **2005**, *30*, 294.
(14) Smith, D. K.; Hirst, A. R.; Love, C. S.; Hardy, J. G.; Brignell, S. V.; Huang, B. *Prog. Polym. Sci*. **2005**, *30*, 220.
(15) Sengupta, S.; Eavarone, D.; Capila, I.; Zhao, G.; Watson, N.; Kiziltepe, T.; Sasisekharan, R. *Nature* **2005**, *436*, 568.
(16) Welch, P.; Muthukumar, M. *Macromolecules* **1998**, *31*, 5892.
(17) Welch, P.; Muthukumar, M. *Macromolecules* **2000**, *33*, 6159.
(18) Welch, P. M. *Nano Lett*. **2005**, *5*, 1279.
(19) Welch, P. M.; Welch, C. F. *Nano Lett*. **2006**, *6*, 1922.
(20) Allen, M. P.; Tildesley, D. J. *Computer Simulation of Liquids*; Clarendon: Oxford, 1987.
(21) For example, see: Wagner, T. H.; Yi, T.; Meeks, S. L.; Bova, F. J.; Brechner, B. L.; Chen, Y.; Buatti, J. M.; Friedman, W. A.; Foote, K. D.; Bouchet, L. G. *Int. J. Radiat. Oncol. Biol., Phys* **2000**, *48*, 1599. Li, S. P.; Ng, K.-L. *Int. J. Mod. Phys. C* **2003**, *14*, 815.
(22) Mansfield, M. L.; Rakesh, L.; Tomalia, D. A. *J. Chem. Phys*. **1996**, *105*, 3245.
(23) Ballauff, M.; Likos, C. N. *Agnew. Chem., Int. Ed* **2004**, *43*, 2998.
(24) Sheng, Y.-J.; Jiang, S.; Tsao, H.-K. *Macromolecules* **2002**, *35*, 7865.
(25) Antonietti, M.; Bremser, W.; Schmidt, M. *Macromolecules* **1990**, *23*, 3796.
(26) Lescanec, R. L.; Muthukumar, M. *Macromolecules* **1990**, *23*, 2280.
(27) Mansfield, M. L.; Klushin, L. I. *J. Phys. Chem*. **1992**, *96*, 3994.
(28) de Gennes, P.-G. *Scaling Concepts in Polymer Physics*; Cornell University Press: Ithaca, NY, 1979.
(29) Giupponi, G.; Buzza, D. M. A. *J. Chem. Phys*. **2004**, *120*, 10290.
(30) Mansfield, M. L.; Douglas, J. F.; Garboczi, E. J. *Phys. Rev. E* **2001**, *64*, 061401.
(31) Found at http://www.stevens.edu/zeno/.
(32) Bosko, J. T.; Prakash, J. R. *J. Chem. Phys*. **2008**, *128*, 034902.
(33) Mecke, A.; Uppuluri, S.; Sassanella, T. M.; Lee, D.-K.; Ramamoothy, A.; Baker, J. R.; Bradford, G. O.; Holl, M. M. B. *Chem. Phys. Lipids* **2004**, *132*, 3.
(34) Rudnick, J.; Gaspari, G. *J. Phys. A: Math. Gen*. **1986**, *19*, L191.